Large Eddy Simulation of Flow around Circular Cylinders on Structured and Unstructured Grids

J. Fröhlich[1], W. Rodi[1], Ph. Kessler[2], S. Parpais[2], J.P. Bertoglio[2], D. Laurence[3]

[1] Institut für Hydromechanik, Universität Karlsruhe, 76128 Karlsruhe, Germany
[2] LMFA UMR 5509, Ecole Centrale de Lyon, 69131 Ecully, France
[3] EDF DER-LNH, 6 quai Watier, 78041 Chatou, France

Summary

The paper presents LES computations of subcritical flow around circular cylinders at $Re = 3900$ and $Re = 140000$. For the former the results obtained with the Finite–Volume code LESOCC employing a structured grid and the Finite–Element code N3S using unstructured tetrahedra are reported. The results obtained with the two codes are compared with each other and with results reported in the literature in order to assess the performance and the potential of the two approaches.

1 Introduction

The flow around bluff bodies is characterized by complex interactions between different phenomena such as boundary layers, separation and reattachment, shear layers, large two– and/or three–dimensional vortical structures, etc. Such flows are relevant for many applications in mechanical, chemical and civil engineering, aerodynamics and other areas. In particular when fluid–structure aerodynamic coupling or aerodynamic noise production is of concern, the unsteady flow has to be determined with high accuracy. Although models based on the Reynolds Averaged Navier–Stokes equations (RANS) have been applied successfully in many practical computations, these tend to fail for flows involving large unsteady vortical structures. Here, the Large Eddy Simulation (LES) technique clearly has a better potential since no model is required for the large flow structures that depend on the individual geometry of the problem. Only the fine–scale turbulence, which has more universal character, needs to be modelled. A comparison of LES and RANS modelling for a certain test problems has been given recently in a series of papers [7], [29], [30], [31].

The circular cylinder in uniform cross flow is a classical example for bluff body flow. Although the geometry is fairly simple the physics are extremely rich and have been investigated in a large number of papers [42]. Since the flow is very sensitive to experimental conditions such as aspect ratio, blockage, end conditions, turbulence level

etc., such a compilation also reveals that the experimental information available is often of limited accuracy (see also the compilation of [11]).

Applying LES to bluff body flows requires calculation of the flow close to the wall. In cases where the geometry exhibits corners, such as for a square cylinder or a cube, the separation is fixed and the solution is less sensitive to modelling in the near wall region. For a round cylinder, in contrast, the separation depends on the details of the attached boundary layer, be it laminar or turbulent. Another aspect is the use of wall functions. These have generally been developed for situations with flat boundaries so that their application to bodies with entirely different shape is a delicate task, in particular when the separation point is not fixed by the geometry. Attempts are currently being made to develop better strategies for near wall regions [1], [10]; the issue is however far from being settled. For the present computations we therefore decided to avoid the need for wall–function modelling. At the Reynolds numbers considered the boundary layer is laminar and resolved with the grid employed. The simulations therefore are of mixed type with high resolution and direct or almost direct simulation close to the wall and coarse resolution and hence LES in the wake. The results of these computations will be used in future work as a basis for the development of improved wall functions.

In the present configuration, as for any complex geometry, the mesh is non–uniform in order to represent the geometry and to achieve sufficient resolution in critical regions. Since in an LES the inherent filter is generally related to the grid used for the computation, the effect of an inhomogeneous discretization is of concern. We have therefore undertaken a set of separate model computations to elucidate this point.

The main part of the paper deals with the calculation of flow around a circular cylinder in the subcritical regime. We have employed two entirely different codes for this task: a structured Finite–Volume code and an unstructured Finite–Element code. The computational results obtained with each method are interesting on their own but it is their detailed comparison which is main novelty of the present work.

2   Computational methods

2.1   Structured Finite Volume method

The code LESOCC (**L**arge **E**ddy **S**imulation **O**n **C**urvilinear **C**oordinates) has been developed in Karlsruhe by Breuer and Rodi [8], [9]. It employs a Finite Volume (FV) discretization with a non–staggered arrangement of variables using momentum interpolation to avoid velocity–pressure decoupling. Any structured orthogonal or non–orthogonal grid can be used. Both, convective and diffusive fluxes are discretized by 2nd order central differences. The time scheme consists of an explicit predictor step by a 3–step Runge–Kutta scheme for the velocities and an implicit corrector step where a Poisson equation is solved for the pressure correction (SIMPLE). The overall time scheme is of 2nd order as the pressure is not updated in each of the Runge–Kutta steps for computational efficiency. Different subgrid–scale models are implemented. One is the Smagorinsky model with van Driest damping near solid walls. Furthermore, several

variants of the dynamic model with the least–squares approach of Lilly are available. They differ in the way of averaging in space and/or time and in the way of clipping negative viscosities. Different wall function models are implemented but have not been employed in the present computations. The code is highly vectorized and has been validated extensively as described in the references cited.

2.2 Unstructured Finite Element method

Unstructured grids have the advantage that complex geometries can be meshed easily and that local, solution–dependent mesh refinement is possible. Very few attempts of such a discretization in LES have been made [18], [2]. The code N3S was initially developed for the RANS equations, using an upwind scheme and a classical Finite Element (FE) discretization on tetrahedra (linear for the pressure, quadratic for the velocity [27]). While applying this code to LES, Rollet–Miet [32] has shown that a centered scheme is preferable to minimize numerical diffusion since the small time-steps, required for physical reasons in the LES context, are more stringent than the stability criteria of the centered scheme. Next, the standard textbook choice of finite elements, that allows far less degrees of freedom for the pressure than for the velocity, was shown unsuitable for LES. Indeed in this context, a collocated arrangement is preferable to capture the small scales of turbulence which exhibit high frequencies in both pressure and velocity. This N3S-LES code [32] has been used in the present study with the following features: centered Adams-Bashford discretization for the non-linear term, and Crank-Nicolson scheme for the diffusion term. Like the velocity, the pressure is discretized by linear trial functions on the smallest elements. Continuity is obtained by a projection method, yielding a Poisson equation for the pressure. Pressure oscillations are eliminated by the Arakawa method. These oscillations, which can be observed when the tetrahedron elements are obtained from a structured rectangular grid, actually vanish completely when the mesh is fully unstructured. The N3S-LES code was developed and tested by P. Rollet-Miet for grid turbulence, channel flow and the flow through a tube bundle (experiment of [36]). This configuration has been found specifically challenging for RANS models in several ERCOFTAC Workshops [35]. In particular the flow from the axis of the wake to the impingement on the next downstream cylinder was badly predicted, the mean flow and especially the Reynolds stresses. Figure 1 shows the good agreement obtained with N3S-LES and the fairly small influence of the subgrid-scale model.

2.3 Investigation of the influence of the filter size

Most subgrid–scale models rely on ideas and concepts that were developed for isotropic homogeneous turbulence. Theoretical works supporting the existing subgrid models are essentially related to analyses performed in terms of energy flux across a spectral cut-off supposed to be constant [19], [13] and [4].

In the case of an LES on a non–uniform grid, turbulence advected by the mean flow experiences a change in the filter width. The response of the subgrid model to this effect has received little attention in the past. It is here addressed using a two-point
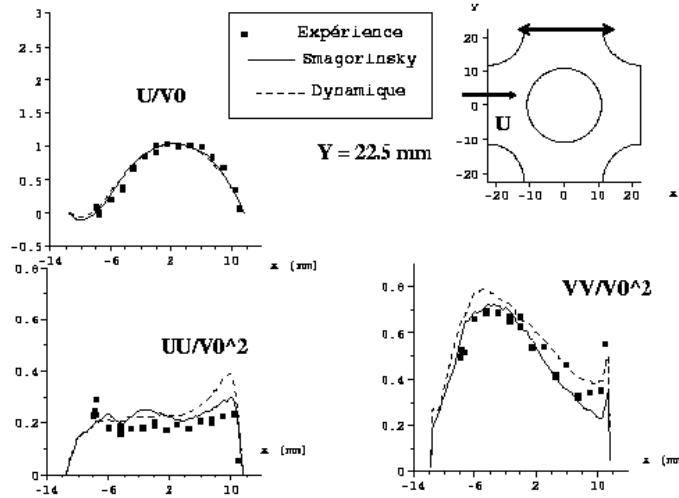
Figure 1 Results of tube bundle computations with N3S obtained with the Smagorinsky model (continuous lines), and the dynamic model (dotted lines). Upper right: geometrical configuration, x and y coordinate in mm. Others: mean and fluctuating velocities versus x at $y = 22.5\ mm$. Symbols indicate experimental values of [36].

closure model (Eddy Damped Quasi-Normal Markovian) extended to inhomogeneous turbulence. The closure model is described in detail in [25]. The main feature of the model is that, at each point of the Reynolds–averaged flow field, a transport equation for the turbulent energy spectrum, $E(K, x)$, is solved. By wave–number integration, the usual turbulent quantities, such as the kinetic energy, can be deduced. For applications to the problem of subgrid models, a wave–number cut–off is introduced, and the effect of small eddies is modeled via a subgrid eddy viscosity. A simple situation is investigated, namely the flow between two flat plates. The wave–number cut–off K_c is supposed to vary with the streamwise direction $K_c = K_c(x_1)$. The channel is divided into three parts. In the first region, ($x_1 < 2.5h$, in Figure 2, where h is half the channel width), the cut–off is uniform and situated at small scales. In the second section ($2.5h < x_1 < 7h$), a much smaller value for K_c is used (5 times smaller), whereas in the last region, K_c is set back to its initial value. Consequently, an abrupt increase in the filter width, followed by an abrupt decrease, are experienced by a fluid particle. The results in Figure 2a show that the mean flow remains nearly unaffected. In Figure 2b, it can be observed that the turbulent kinetic energy decreases in the large filter width region, which is simply related to the fact that there is less energy captured in the resolved field. A more refined analysis, in terms of spectra, shows that the large scales are left nearly unaltered in this case.

When the flow re–enters the fine–resolution domain, the turbulent kinetic energy is overestimated. The explanation is that, the cut–off being suddenly shifted to a higher wave–number, it takes some time before the spectrum recovers an equilibrium state. During this time, the dissipation is underestimated, inducing the overestimation of the

turbulent kinetic energy. Further investigations are necessary before definite conclusions can be reached: a more realistic geometry and more progressive variations in the filter width should be introduced. However, the present results already provide an optimistic information concerning LES of wakes, the worse situation being encountered when the eddies are advected from a coarse mesh region to a more refined zone, which is not the case in the flow around a cylinder where turbulence is essentially generated on a fine mesh and then advected to a coarser mesh region.
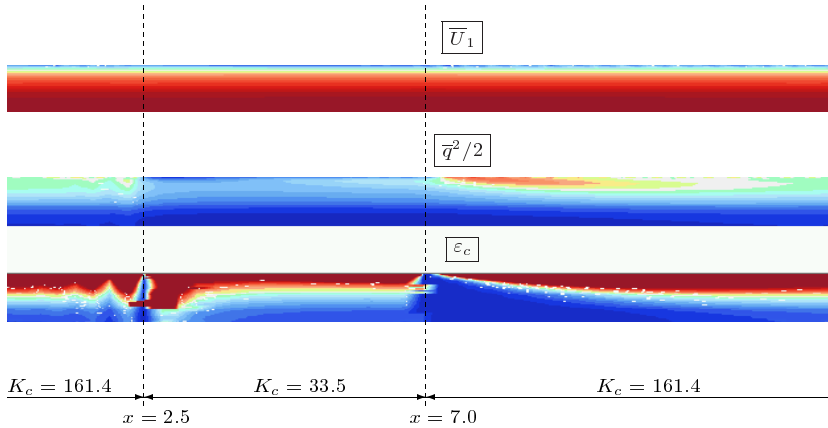

Figure 2   Channel flow with spatially varying filter (sharp spectral cut-off $K_c(x_1)$), only the upper half of the domain is shown.

3   Results for the circular cylinder

3.1   Various flow regimes and choice of Reynolds number

The large amount of literature on the flow around circular cylinders is reviewed in detail in the recent book of Zdravkovich [42]. Different regimes are observed depending on the Reynolds number $Re = Du_\infty/\nu$ where D is the cylinder diameter, u_∞ the free stream velocity and ν the kinematic viscosity. The two Reynolds numbers selected for the computations below both belong to the subcritical regime ($Re = 350 - 200000$). In this regime the boundary layer on the cylinder wall extending from stagnation point to separation point is laminar while the transition to turbulence occurs after a transition length L_t in the shear layer which forms behind the separation point. Further downstream these vortices roll up to form the larger, alternating von Karman vortices. This alternate shedding causes the boundary layer and the stagnation point to oscillate accordingly [26].

The subcritical regime can further be divided into a lower (up to $Re = 1500$), an intermediate ($Re = 1500 - 30000$), and an upper subcritical regime (above $Re = 30000$). In the intermediate regime the shear layer persists for a while after separation before it becomes unstable due to Kelvin–Helmholtz type vortices and spanwise instability. With increasing Reynolds number the transition length L_t decreases from $1.5D$ to $0.2D$, i.e. it takes place immediately after separation, while the formation length changes from $2.5D$ to about $1D$ [42]. The three–dimensional structure of the near wake has been visualized in e.g. [39] and investigated in [14], [15] by measurement of the streamwise vorticity component. Computations of the correlation lengths of this quantity for $Re = 5000$ in spanwise and cross–stream direction yield minimum values of $\lambda_z = 0.55D$ and $\lambda_y = 0.1D$ close to the separation point, respectively, both increasing in streamwise direction [14]. The ratio λ_z/λ_y corresponds to the one observed for mixing layers [15] suggesting that the mechanisms involved are similar.

In the upper subcritical regime the time–averaged flow changes only little with Re. As in the intermediate regime the flow exhibits considerable three–dimensionality . Variations of the flow also occur from cycle to cycle, so that e.g. the Strouhal number may temporarily differ from the mean by as much as 10% with drag and lift varying accordingly. Detailed phase–averaged measurements of the near wake at $Re = 140000$ have been published in [11].

The Reynolds numbers $Re = 3900$ and $Re = 140000$ have been selected for the LES computations below for the following reasons. The lower one was studied in some detail by LES performed at the CTR, Stanford, [3], [21], [22]. It allows a comparison with these results and also with the experiments in [24]. Breuer [6] also investigated this flow in independent computations with LESOCC focussing particularly on the influence of the convection scheme and the subgrid–scale model. The higher Reynolds number was chosen because only for this value detailed phase–resolved experimental data are available for comparisons [11]. Up to now no successfull LES has been published for this case. Such higher Reynolds numbers are more relevant for applications since they are frequently encountered in chemical, mechanical, and nuclear engineering [42].

3.2 Boundary conditions and mesh

The coordinate system is oriented such that x designates the streamwise, y the normal, and z the spanwise coordinate, respectively. All lengths are normalized with the cylinder diameter D, whereas velocities are nondimensionalized with the freestream velocity. Angles are counted from the upstream average stagnation point.

For the structured grid used by LESOCC we employed a circular computational domain with radius 15. It allows to use an O-mesh, depicted in Figure 3, which is advantageous due to its constant quality all along the cylinder wall. (Previous RANS computations in [5] have shown that with an H-mesh inadequate resolution close to the stagnation point considerably affected the result.) The points are clustered in the wake and near the wall using geometric stretching [8], [6]. A laminar inflow condition was employed for $x < 0$, i.e. $u = 1$, $v = w = 0$. The outflow boundary condition was a convective one. In spanwise direction we used periodic conditions with period length
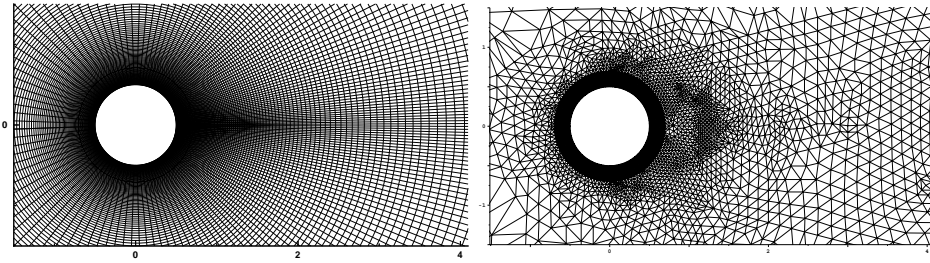
Figure 3 Grid for computations at $Re = 3900$ in the $x - y$-plane, identical zoom near the cylinder. Left: structured FV grid for LESOCC, right: unstructrued FE grid for N3S.

π, the same as in [3]. A no–slip condition was applied at the cylinder wall. The mesh consists of $N_i = 166$ points in radial, $N_j = 166$ in circumferential, and $N_k = 32$ or $N_k = 48$ in spanwise direction, respectively, yielding a total of 881792 and 1322688 points. (The effective number of unknowns is smaller as in directions of periodicity 6 points are employed to implement this condition.) Three computations employing the Smagorinsky model were performed at $Re = 3900$: LRUN1: $N_k = 32$, $C_s = 0$, i.e. no SGS–model, LRUN2: $N_k = 32$, $C_s = 0.1$, LRUN3: $N_k = 48$, $C_s = 0.1$.

The grid for the N3S computations was constructed after the first results with LESOCC had been obtained which allowed to benefit from the available information. The computational domain was chosen to be a rectangular box with $x \in [-5, 15]$, $y \in [-5, 5]$, $z \in [0, \pi]$. This implies a blockage ratio of 0.1 which is higher than for the circular domain but still comparable to most of the experiments [42]. The unstructured grid employs thetraedral elements and was set up in a zonal way. A two–dimensional grid comprising an annulus of thickness 0.1 (20×120 equidistant points) and a V–shaped domain of unstructured triangles covering the wake was constructed. This grid was repeated in 39 parallel planes in spanwise direction and completed to yield a tetrahedral mesh. The remaining space was filled with a fully 3d Voronoï triangulation so that the final grid contains 176286 points. As for the structured code, the inflow condition was laminar, the outflow condition was a convective one, and periodicity was imposed in the spanwise direction. A slip condition was used on the lateral boundaries. For the wall boundary condition the wall function approach of Werner and Wengle [40] was used. However, the mesh is sufficiently fine so that this condition is actually applied in the viscous sublayer. Since in this region a linear velocity distribution is assumed the wall function becomes effectively a no–slip condition. The same subgrid–scale model was employed as with the structured code, namely the Smagorinsky model with $C_s = 0.1$.

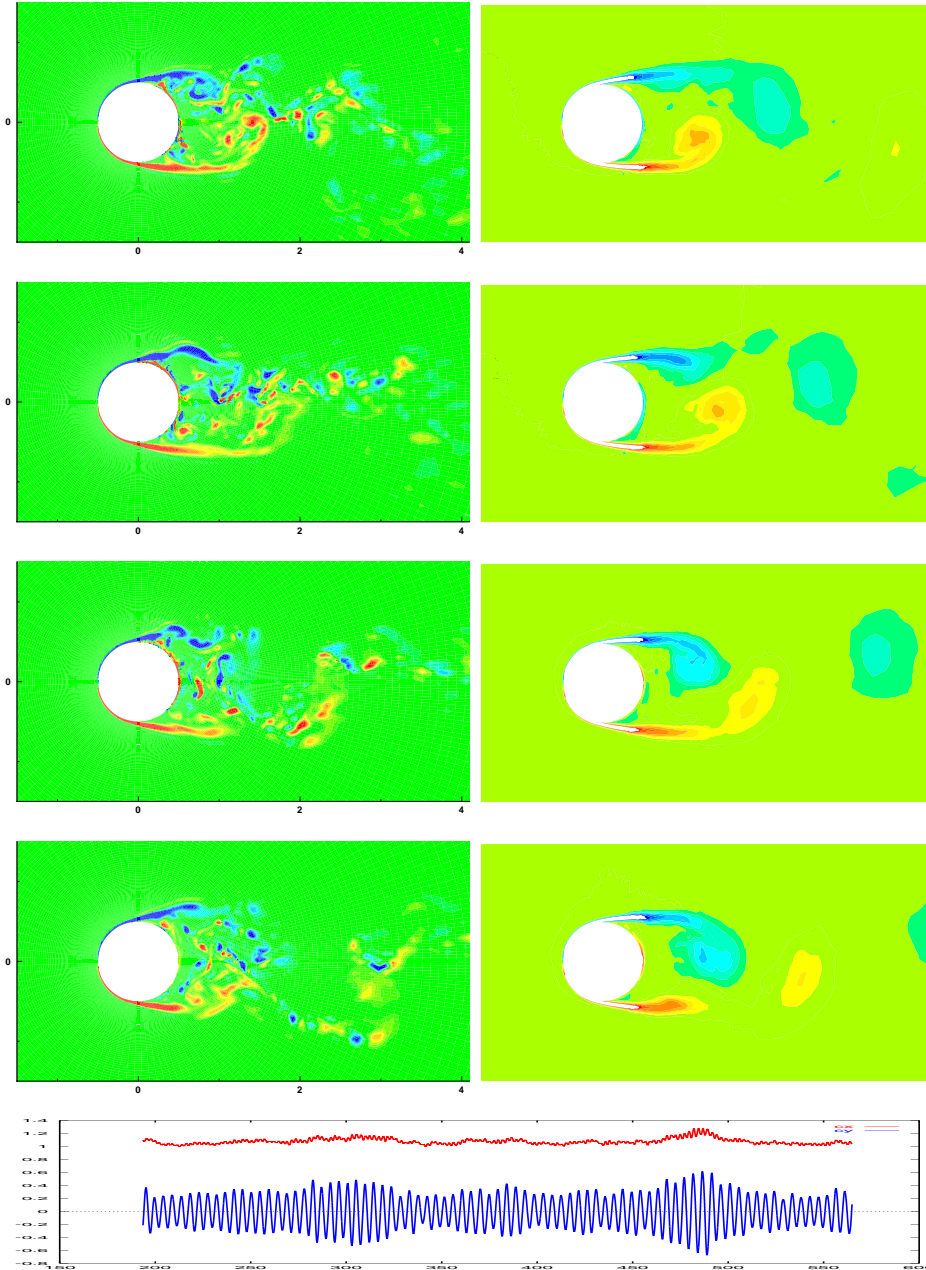A zoom of both grids in the vicinity of the cylinder is shown in Figure 3.

Figure 4 Axial component of the vorticity vector for $Re = 3900$. Left: LRUN2, $\Delta t_{frame} = 0.96$, right: NRUN1, $\Delta t_{frame} = 1$. Bottom window: Time record of drag coefficient C_D (top) and lift coefficient C_L (bottom), in LRUN2 over 80 shedding cycles.
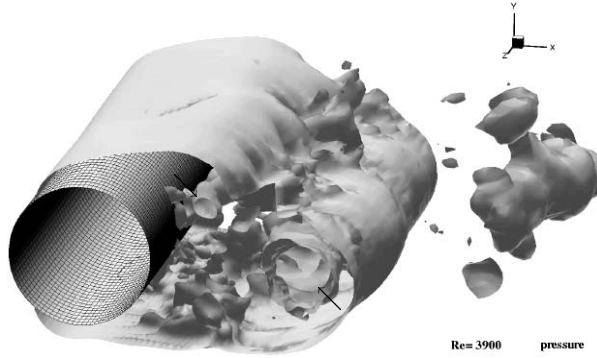
Figure 5 Instantaneous pressure surfaces at $p = -0.34$ and $p = -0.67$, respectively. The latter represents two rolls inside the former (arrows), the remaining plot corresponds to the higher value.

3.3 Instantaneous flow field

This section and 3.4–3.6 are concerned with the results for $Re = 3900$. We compare the solutions obtained with the structured and unstructured method and results reported in the literature.

In order to give an impression of the computed time–dependent solution of the LES with both methods, Figure 4 displays the axial component of the instantaneous vorticity vector in a cut normal to the cylinder axis at similar time intervals. Due to the highly three–dimensional and irregular flow which will be further highlighted below it is of course impossible to obtain virtually corresponding plots. Even from one period to another the solution is different in the same computation. We note that the computed solution corresponds very well to the physical description of the flow given above. In particular, the shear layers forming after separation can be discerned as well as their breaking up into smaller vortices. The larger von Karman vortices are also visible. In the figure, one of them travels to the lower right corner while a second one forms on the upper side. It is also obvious that, due to different grid scales in the two computations, the granularity of the solution is higher in the FV computation than for the FE solution. The large vortices, however, are similar.

The bottom frame of Figure 4 contains a plot of drag and lift coefficient obtained with the structured code. The oscillations are quite regular with respect to their period. The magnitude of the oscillations reflects the spanwise correlation and depends on the length of the cylinder (see [41] for a study at somewhat higher Re.) The modulation of the amplitude, on the other hand, is no deficiency of the computation but is observed similarly in experiments [38] [42]. This irregularity is due to in the irregular three–dimensional break up of the vortices. This is highlighted in Figure 5 displaying two instantaneous iso–pressure surfaces in the FV computation. The figure shows particularly well the instability of the shear layer in spanwise direction resulting from the mechanism of secondary vortices proposed in [39].
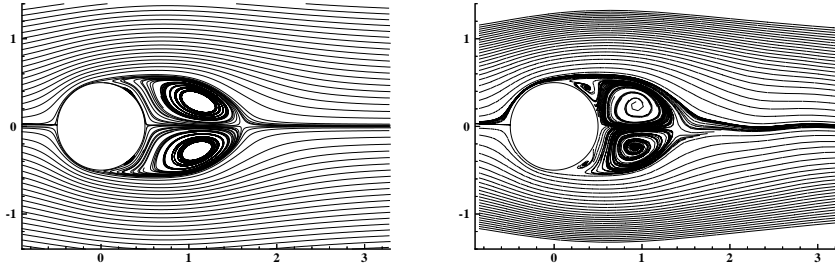
Figure 6   Average stream lines of LRUN3 (left) and NRUN1 (right).

The considerable three–dimensionality of the wake flow is further reflected by the spanwise velocity component (not shown here). In the center plane ($y = 0$) its extrema exceed 70% of the free stream velocity.

3.4   Mean flow and global quantities

After a suitable start–up phase, the flow field has been averaged with respect to the spanwise coordinate and in time (20 cycles for NRUN1 and 86 cycles for LRUN3). The resulting quantities are denoted by brackets. Streamlines of the two–dimensional average flow are presented in Figure 6. Apart from the large recirculation zone behind the cylinder, two small secondary recirculation zones are obtained with LRUN3. These have been obtained in [3] as well and are reported in [37] to exist at $Re = 5000$. In the results of NRUN1 the secondary recirculation zones appear to be more pronounced.

Figure 7a displays the mean streamwise velocity along the centerline. Comparing the curves for NRUN1 and LRUN3 reveals that the former is not very smooth in the far wake which is a consequence of the coarse grid employed in this region as well as the shorter averaging time. The recirculation length is underpredicted in NRUN1. The curve of LRUN3 agrees fairly well with the experiment [20] in the recirculation zone and with the data of [24] in the wake (the data of [20] seem to be questionable around $x = 3$). The other parts of Figure 7 contain lateral profiles at $x = 1.54$, i.e. close to the end of the mean flow separation point in Figure 6. The result of LRUN3 matches the streamwise velocity of the experiment while NRUN3 yields a positive value of the mean velocity, a consequence of the shorter recirculation length. It should be noted that at $y = \pm 5$, the border of the computational domain in NRUN1, $< \bar{u} >= 1.06$ while in LRUN3 $< \bar{u} >= 1.03$ and is decreasing further in the outward direction. This amount of acceleration due to blockage seems acceptable. Figure 7c also displays profiles of $< \bar{v} >$ at $x = 1.54$. The extrema appear at the edges of the mean recirculation bubble and are larger in the present computations than measured in the experiment. Note however that the experimental data exhibit uncertainty monitored by the unsymmetry of the measurements [3].

Figure 7 also compares the present results to those of [3] obtained with a staggered discretization of $144 \times 136 \times 48$ cells. We have included the curves obtained with the
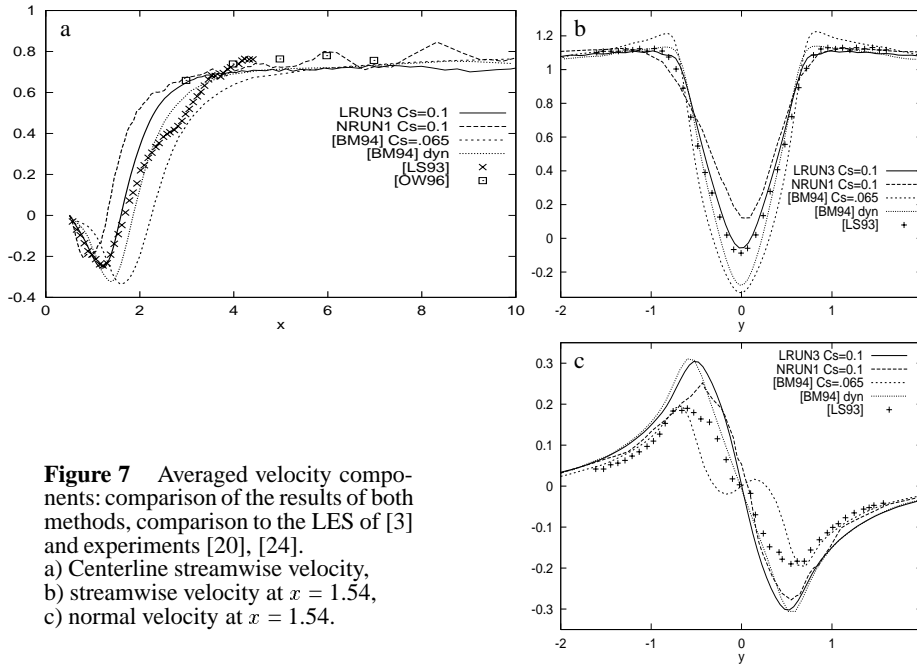
Figure 7 Averaged velocity components: comparison of the results of both methods, comparison to the LES of [3] and experiments [20], [24].
a) Centerline streamwise velocity,
b) streamwise velocity at $x = 1.54$,
c) normal velocity at $x = 1.54$.

Smargorinsky model ($C_s = 0.065$) as well as those computed with the dynamic model since the latter were the most satisfactory in that reference. The mean recirculation length is predicted considerably higher in these computations than in the present ones which agree fairly well with the experimental data. The more reliable of the two $< \bar{v} >$ profiles is very close to the present results.

Table 1 supplements the above comparisons with more quantitative data: the Strouhal number agrees very well with the experimental results. However, in the regime considered here this quantity is relatively insensitive to the details of the calculation. A similar observation has been made for the square cylinder [31]. The drag coefficient is slightly overpredicted in the results of LESOCC. This is related to a somewhat higher separation angle (but still $\Theta < 90°$) and a lower base pressure. The former also yields a shorter recirculation length. These observations illustrate the interaction between the upstream boundary layer and its separation with the downstream recirculation zone. With the N3S code, the drag coefficient is overpredicted significantly more.

3.5 Influence of subgrid–scale model and spanwise discretization

Figure 9 compares the three runs with LESOCC listed in Table 1. With respect to the case LRUN2 the influence of the subgrid–scale model can be assessed by comparing to LRUN1, whereas the influence of the spanwise discretization is revealed by comparison to LRUN3. These results have been obtained in parallel to [6] to which the reader
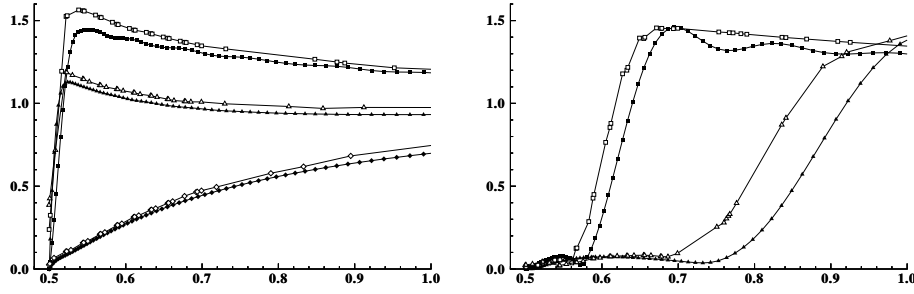
Figure 8 Radial profiles of the absolute value of the mean velocity vector. Solid symbols: LRUN3, cell centers in the structured FV mesh, hollow symbols: NRUN1, intersections of the cut with element faces in the FE mesh. Left: profiles through the attached boundary layer at $2°(\diamond)$, $41°(\triangle)$, $80°(\square)$, respectively, Right: profiles at $114°(\square)$, and $138°(\triangle)$, respectively, where the boundary layer has separated.

Table 1 Global quantities for cylinder flow comptations at $Re = 3900$, comparision of the present results to LES of Beaudan, Moin [3] as well as to the experiments: St= Strouhal number, C_D= drag coefficient, C_{bp}= back pressure coefficient, Θ= separation angle in degrees, L_r= length of recirculation zone.

	N3S	LESOCC			BM [3]		Experiment
	NRUN1	LRUN1	LRUN2	LRUN3	n.m.	Smag.	
St	0.216	0.210	0.210	0.216	0.216	0.209	0.215 ± 0.005 [12]
C_D	1.45	1.17	1.08	1.08	0.96	0.92	0.98 ± 0.05 [23]
C_{bp}	-1.59	-1.15	-1.06	-1.03	-0.89	-0.81	-0.90 ± 0.05 [23]
Θ	90.0	89.0	88.0	88.1	85.3	84.8	85 ± 2 [37]
L_r	0.80	0.96	1.09	1.09	1.56	1.74	1.33 ± 0.2[12], 1.19[20]

is refered for further discussion, in particular concerning the effect of different convection schemes. Figure 9a shows the turbulent kinetic energy. It rises steeply behind the cylinder and attains its maximum near the end of the main recirculation zone. The small difference between the computations with and without subgrid–scale model reflects the amount of energy contained in the subgrid–scales. Due to the typical decay of the spectral energy this portion is naturally limited since the large, energy–containing vortices are resolved. On the other hand, inspection of Table 1 indeed shows that the solution changes only little between LRUN1 and LRUN2.

The same holds for the Reynolds stress components shown in Figure 9b and 9c. Note that the streamwise gradient of k is fairly high. Since its principal contribution is the Reynolds stress $< \bar{v}'\bar{v}' >$, the profiles of this quantity at $x = 1.54$ are very sensitive to streamwise dislocations in the flow field. An increase in spanwise resolution improves the result concerning the global quantities in Table 1. It yields slightly increased

Reynolds stresses which is simply due to a shift of the cut–off scale to higher wave numbers in spanwise direction. It is interesting to note, however, that closely behind the cylinder the turbulent kinetic energy decreases further.

We conclude that the results in this section show that the subgrid–scale model and the spanwise discretization are of similar importance in for the present computation. This is in accordance with [3] [6] and [22]. It led to the implementation of a Fourier discretization for the z-direction in the last reference.
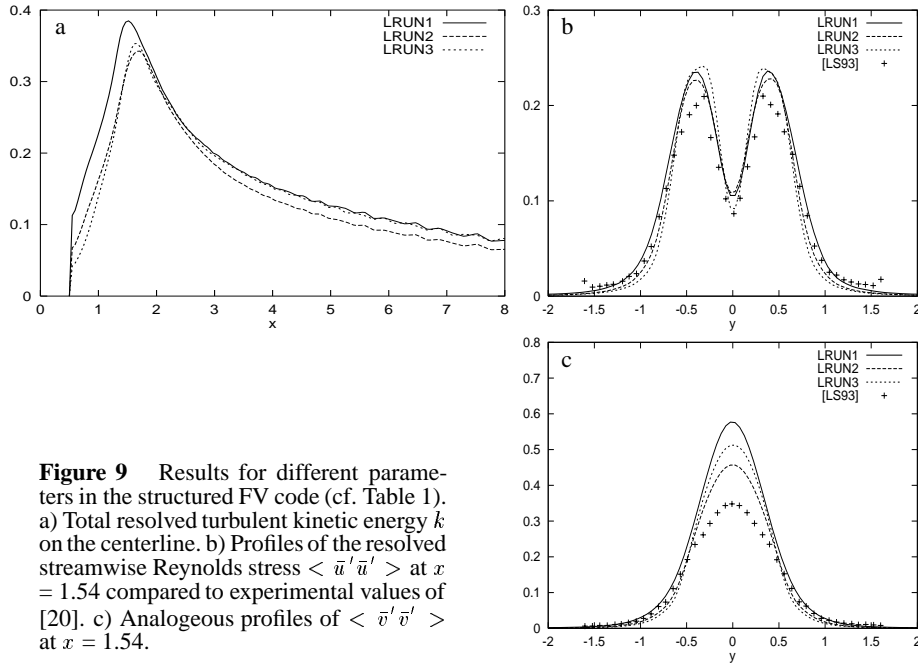

Figure 9   Results for different parameters in the structured FV code (cf. Table 1). a) Total resolved turbulent kinetic energy k on the centerline. b) Profiles of the resolved streamwise Reynolds stress $< \bar{u}'\bar{u}' >$ at x = 1.54 compared to experimental values of [20]. c) Analogeous profiles of $< \bar{v}'\bar{v}' >$ at $x = 1.54$.

3.6   Comparison of resolution and computational effort

The resolution of the laminar boundary layer along the upstream cylinder wall requires a fine mesh in radial direction. This also limits the azimuthal mesh size for numerical reasons. On the rear side a small radial mesh size is less important. The wake can be discretized with an increasingly coarser mesh towards the outflow boundary. The employed structured grid employed in LESOCC meets the above resolution requirements. The radial cell size near the cylinder wall is $\Delta r_1 = 0.0025$ yielding $max\{y_1^+\} \approx 1$. Radial profiles of the absolute value of the velocity vector in Figure 8 illustrate the boundary layer resolution.

With an unstructured grid the discretization can be adapted better to the flow considered. In the present case a grid with about 7.5 times fewer points than the structured

grid was employed. In particular the upstream region can be resolved more efficiently. Note that a coarsening of the grid in spanwise direction can easily be achieved in regions where the flow is known to be almost two–dimensional. The elements adjacent to the wall are of size $\Delta r_1 = 0.005$, similar to [3]. Radial profiles of the average solution are displayed in Figure 8. Comparing the curves for the two computations we notice the slight acceleration due to the different domain size mentioned above. The curves at larger angles are quite sensitive to the actual form of the recirculation bubble. Those of NRUN1 are to the left of the companion ones due to the slightly larger separation angle. The symbols in Figure 8 reflect the respective discretization. It is somewhat finer in the structured grid with, e.g., 28 instead of 20 points within a distance of 0.1 from the cylinder wall. However, the difference is not as drastic as it might appear. The symbols representing the intersection with the element faces are clustered and, e.g., the shear layer at $\theta = 114°$ is discretized with 19 and 16 points, respectively. An interesting feature is the increased smoothness of the mean velocity with N3S particularly visible at $\theta = 114°$. Note that this is a location where the flow is still laminar. The oscillations persisting in the average are presumably due to the existence of a prefered direction in the structured mesh, whereas this radial anisotropy is not present in the bulk of the FE mesh (cf. Figure 3). Finally, the discussion in Section 3.5 and the results of [21], [22] and [6] show that sufficient resolution in spanwise direction is important. The higher the number of points on the cylinder wall in this direction, the larger is the potential saving with an unstructured discretization.

Comparing the performance of two entirely different codes run on different machines is of course a delicate task and can only result in gross estimates. Note for example that N3S is a complex general purpose code whereas LESOCC is "streamlined" for the present task. The price to be paid for the saving of grid points with an unstructured discretization is a higher complexity of the code and a larger CPU time per point. The advantage of this approach highly depends on the flow considered and the particular discretization. The results presented were obtained with LESOCC at 620 MFLOPS on a VPP300[1] and with N3S at 440 MFLOPS on a CRAY98[2]. The CFL number was $0.7-1$ for LRUN3 and 0.3 for NRUN1. One time step of LRUN3 took $9.3\,sec$ and $18\,sec$ in NRUN1. Taking into account the different FLOP–rate the performance of both codes is similar for the present case. For higher spanwise resolution or problems with more complex geometry the unstructured method is likely to be more efficient.

3.7   Results for Re = 140000

The Reynolds number considered is in the upper subcritical regime: the boundary layer on the cylinder is still laminar, but the transition to turbulence takes place very shortly after separation. For slightly higher values, i.e. around $Re = 2 - 3 \times 10^5$ the boundary layer becomes turbulent, the Strouhal number increases and the well–known drag crisis is observed. Hence, at the border of the upper subcritical regime the flow is fairly sensitive to disturbances in experimental or numerical conditions [11] [28].

---

[1] Rechenzentrum Universität Karlsruhe
[2] IDRIS (Institut du Développement et des Ressources en Informatique Scientifique) and EDF, Paris.
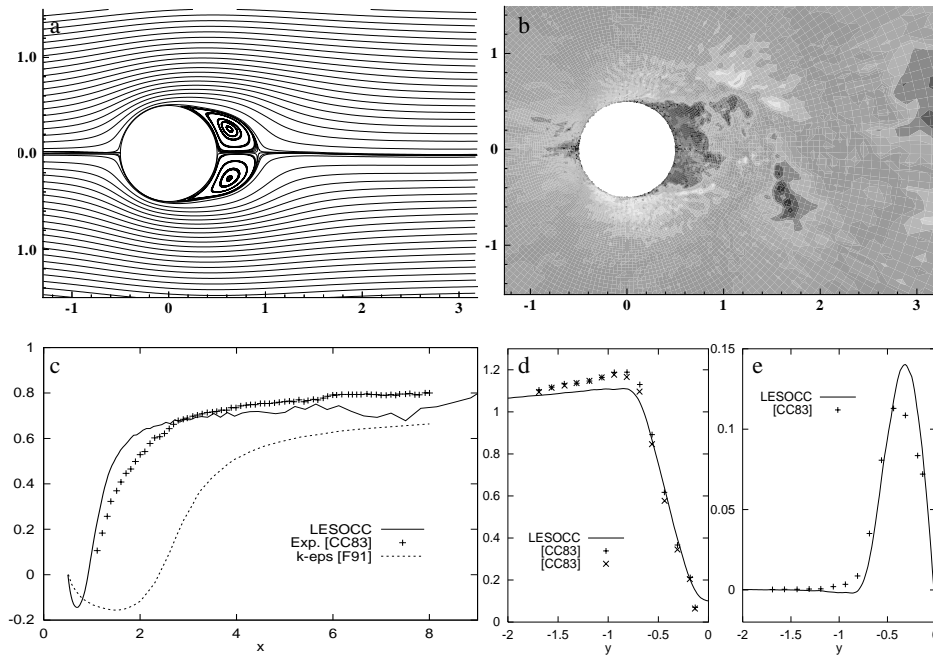
Figure 10 Results for the cylinder flow at $Re = 140\,000$: a) streamlines of the mean flow, b) magnitude of the instantaneous velocity in a plane normal to the cylinder axis, the maximum is about 2.25, c) mean streamwise velocity at $y = 0$, d) mean streamwise velocity at $x = 1$, e) resolved shear stress $< \bar{u}'\bar{v}' >$. Symbols indicate measured total shear stress from [11] obtained by adding phase–averaged and random contribution.

The flow was computed with LESOCC and a no–slip condition on the wall. Since the boundary layer thickness behaves like $1/\sqrt{Re}$ [34] the grid spacing should be smaller by a factor of 6 than in the computations above to achieve the same quality of resolution. It is clear, however, that this cannot be obtained with the available means. Reducing the minimal mesh size in radial direction is relatively easy due to the exponential behaviour resulting from the geometric stretching employed. On the other hand, the mesh size decreases only linearly with the number of points in azimuthal and spanwise directions. After extensive two–dimensional tests we used a grid with $166 \times 206 \times 64$ points in radial, azimuthal, and axial direction, respectively. Radial stretching of 4.5% yields $\Delta r_1 = 4.8 \times 10^{-4}$, and the cells were evenly spaced on the cylinder wall in all directions. Experimental results in [42] suggest that the spanwise correlation length is significantly lower in the present regime than for $Re = 3900$ so that we set the spanwise period length to 1. The diameter of the computational domain is 15. The Smagorinsky model was applied with $C_s = 0.1$ and the computation was started from uniform flow. After about 7 shedding periods the statistical quantities were assembled during 16 periods.

Figure 10 collects some of the results. The plot of the instantaneous velocity illustrates the extremely narrow boundary layer and shear layer, the fine scale structures in the wake, as well as spurious oscillations on the sides. The recirculation length is much smaller than for the lower Reynolds number, and no secondary recirculation zone is observed. In this context it is interesting to note that in [37] a secondary vortex with angular extent of $12°$ was observed for $Re = 10^5$. The velocity gradient from which this was infered can however also result from spanwise flow since the employed device is insensitive to direction. Indeed, the three–dimensionality of the flow is considerable (see Figure 11). The spanwise velocity component locally exceeds 0.9. In Figure 10 we observe that the recirculation length matches the experimental data (the value in Table 2 is obtained from flying–hot–wire data which are less reliable very close to the cylinder [11]). Comparing the velocity on the centerline reveals that $< \bar{u} >$ is overpredicted closely behind the recirculation bubble while being slightly too small around 6 diameters from the cylinder. In the latter region, however, the grid is already quite coarse and the averaging could be improved. Nevertheless, the agreement is quite good. The normal profile of $< \bar{u} >$ in Figure 10d also shows the relatively good agreement with the experiment. Figure 10e finally reports the resolved shear stress $< \bar{u}'\bar{v}' >$, which also agrees satisfactorily. On the other hand, Figure 10a and Table 2 show that the separation angle is too large in the computation. This goes along with a slightly lower drag. The Strouhal number is within the experimental range but relatively large while the back pressure coefficient agrees fairly well. Our interpretation, backed by the wavy streaklines upstream of the separation in Figure 11, is the following: as discussed above the discretization of the boundary layer is relatively coarse (at certain instances the value of y_1^+ locally exceeds 5 in the front part). This induces additional numerical oscillations so that the boundary layer experiences additional "turbulence" as if the Reynolds number were somewhat larger. Indeed, the backward shift of the separation, reduced drag, and increase in Strouhal number all point to a premature tendency towards the critical state.

Finally, we can make a comparison with previous results obtained with statistical models. Figure 10c includes the corresponding curve obtained with a two–layer $k - \epsilon$ turbulence model [16]. It is evident that the model gives unsatisfactory results for the considered flow. This is due to the presence of large scale fluctuations which are known to be difficult to model by RANS methods; in particular the $k - \epsilon$ model underpredicts the strength of the periodic shedding motion.

Table 2 Global quantities for cylinder flow computations at $Re = 140000$.

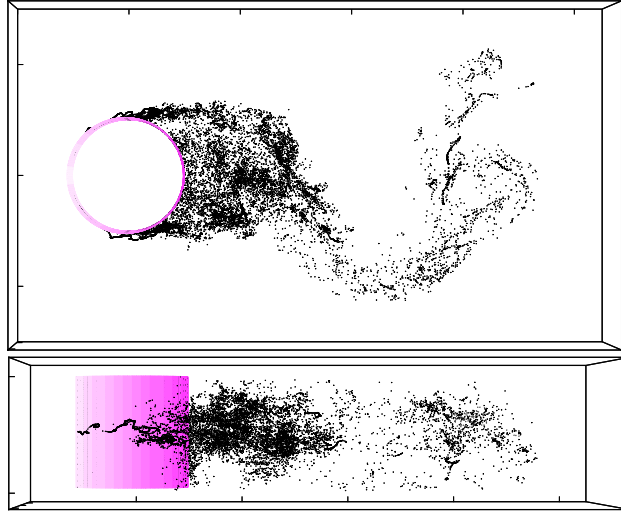|	St	C_D	C_{bp}	L_r/D	Θ
LESOCC	0.217	1.157	−1.33	0.42	93.8
Experiment [11]	0.179	1.237	−1.21	0.5	
[33],[38],[37]	0.2	1.2	−1.34		79

Figure 11 Streaklines in the computation at $Re = 1400000$ starting at two points close to the stagnation line, top and side view at the same instant. The figures show a closeup near the cylinder, tics are placed at unity distance. In the top view the streaklines are partly covered by the representation of the cylinder wall.

4 Conclusions

The paper reports on large-eddy simulations of flow around circular cylinders at two different subcritical Reynolds numbers. The complex physical phenomena occurring in these flows are generally well captured by the calculations and the results agree favourably with experiments. It is the first time that such calculations are reported for the high Reynolds number of Re = 140000; also in this case the results are in most respects satisfactory, but the very thin laminar boundary layer up to separation could not be resolved sufficiently and a better treatment of this boundary layer should be attempted. Altogether, the results show clearly that LES is much more suitable for simulating this type of flow than are RANS models.

A special effort was made to compute the case with Re = 3900 under similar conditions with a structured FV code and an unstructured FE code in order to allow a detailed comparison of the two methods. First of all, the results demonstrate that the unstructured LES code is operational and LES calculations are possible with unstructured FV methods. The comparison has shown that both codes run at similar cost for the case computed: the extra computational effort due to the unstructured nature of the code is roughly compensated by the lower number of grid points that need to be used. However, the comparison of the results also revealed that, in the case of the unstructured grid employed, the reduction of grid points was overdone somewhat as the separated shear layer and the wake were not resolved sufficiently.

Proper construction of a suitable grid for LES calculations of complex flows is a difficult task for both structured and unstructured grids. While the former suffer from the introduction of unnecessary points in certain areas, the latter require a priori knowledge on where fine resolution is necessary and hence on what an ideal discretization should look like. Only with substantially fewer grid points does the higher price per grid point pay off when the unstructured method is used. Hence, great effort has usually to be invested in generating a suitable mesh. In the case of structured grids, better economy with regard to grid points can be achieved by using block-structured grids; this technique is currently implemented into LESOCC.

In any case, with a fixed mesh good a priori knowledge on the properties of the solution is required. However, often such knowledge is lacking and it is increasingly difficult to obtain the more complex the flow situation is. When using an unstructured grid, the natural way out of this dilemma is of course to employ a method that allows to adapt the grid during the calculation, based on certain quality criteria. Certainly, much work is still required in developing such adaptive mesh techniques suitable for large-eddy simulations.

Acknowledgment

References

[1] E. Balaras, C. Benocci, and U. Piomelli. Two-layer approximate boundary conditions for large–eddy simulations. *AIAA*, 34:1111–1119, 1996.

[2] F. Bastin. Jet noise using LES. In *Annual Research Briefs 1996*, Center for Turbulence Research, 1996.

[3] P. Beaudan and P. Moin. Numerical experiments on the flow past a circular cylinder at sub–critical Reynolds number. Technical Report TF-62, Stanford University, 1994.

[4] J.P. Bertoglio and J. Mathieu. Study of subgrid models for sheared turbulence. *4th Symposium on Turbulent Shear Flows, Karlsruhe*, 1983.

[5] G. Bosch. *Experimentelle und theoretische Untersuchung der instationären Strömung um zylindrische Strukturen*. PhD thesis, Universität Karlsruhe, 1995.

[6] M. Breuer. Numerical and modelling influences on large eddy simulations for the flow past a circular cylinder. In *Proceedings of the 11th Turbulent Shear Flow Conference, Sept. 8-11, 1997, Grenoble, France*, 1997.

[7] M. Breuer, D. Lakehal, and W. Rodi. Flow around a surface mounted cubical obstacle: Comparison of LES and RANS–results. In M. Deville, S. Gavrilakis, and I.L. Ryming, editors, *Computation of 3D Complex flows*, volume 53 of *Notes on Numerical fluid Mechanics*, pages 22–30. Vieweg Verlag, 1996.

[8] M. Breuer and W. Rodi. Large eddy simulation of turbulent flow through a straight square duct and a 180° bend. In P.R. Voke, R. Kleiser, and J.P. Chollet, editors, *Fluid Mech. and its Appl.*, volume 26. Kluwer Acad. publ., 1994.

[9] M. Breuer and W. Rodi. Large eddy simulation of complex turbulent flows of practical interest. In E.H. Hirschel, editor, *Flow simulation with high performance computers II*, volume 52 of *Notes on Numerical Fluid Mechanics*, pages 258–274. Vieweg, Braunschweig, 1996.

[10] W. Cabot. Near–wall models in large eddy simulations of flow behind a backward facing step. In *Annual Research Briefs 1996*, pages 199–210. Center for Turbulence Research, 1996.

[11] B. Cantwell and D. Coles. An experimental study of entrainment and transport in the turbulent near wake of a circular cylinder. *J. Fluid Mech.*, 136:321–374, 1983.

[12] G.S. Cardell. *Flow past a circular cylinder with a permeable splitter plate*. PhD thesis, Graduate Aeronautical Lab., California Inst. of Technology, 1993.

[13] J.P. Chollet and M. Lesieur. Parameterization of small scales of three dimensional isotropic turbulence. *J. Atmos. Sci.*, 38:2747–2757, 1981.

[14] C.K. Chyu. *A study of the Near–Wake Structure from a Circular Cylinder*. PhD thesis, Lehigh University, Bethlehem, Philidelphia, USA, 1995.

[15] C.K. Chyu and D. Rockwell. Evolution of patterns of streamwise vorticity in the turbulent wake of a circular cylinder. *J. Fluid Mech.*, 320:117–137, 1996.

[16] R. Franke. *Numerische Berechnung der instationaeren Wirbelablösung hinter zylindrischen Körpern*. PhD thesis, Universität Karlsruhe, 1991.

[17] K. Jansen. (private communication).

[18] K. Jansen. Unstructured grid large eddy simulation of wall bounded flows. Annual Research Briefs, 1993.

[19] R.H. Kraichnan. Eddy viscosity in two and three dimensions. *J. Atmos. Sci.*, 33:1521–1536, 1976.

[20] L.M. Lourenco and C. Shih. Characteristics of the plane turbulent near wake of a circular cylinder. A particle image velocimetry study. (data taken from Beaudan,Moin(1994)), 1993.

[21] R. Mittal. Large–eddy simulation of flow past a circular cylinder. In *Annual Research Briefs 1995*, pages 107–116. Center for Turbulence Research, 1995.

[22] R. Mittal. Progress of LES of flow past a circular cylinder. In *Annual Research Briefs 1996*, pages 233–241. Center for Turbulence Research, 1996.

[23] C. Norberg. Effects of Reynolds number and low–intensity free–stream turbulence on the flow around a circular cylinder. Technical Report Publ. No. 87/2, Dep. of Appl. Thermosci. and Fluid Mech., Chalmers Univ. of Technology, Sweden, 1987.

[24] L. Ong and J. Wallace. The velocity field of the turbulent very near wake of a circular cylinder. *Experiments in Fluids*, 20:441–453, 1996.

[25] S. Parpais and J.P Bertoglio. A spectral closure for inhomogeneous turbulence applied to turbulent confined flow. 6th European Turbulence Conference, Lausanne, 1996.

[26] D.E. Paxson and R.E. Mayle. Velocity measurements on the forward portion of a cylinder. *J. Fluids Eng.*, 112:243–245, 1990.

[27] G. Pot, L.L. de Sousa, J.P. Gregoire, and Y. Souffez. Improvement of industrial finite element algorithms for CFD code N3S. In Morgan, Onate, Periaux, Peraire, and Zienkiewicz, editors, *Finite Elements in Fluids*, volume 1, pages 527–536. Pineridge Press, 1993.

[28] A. Richter and E. Naudascher. Fluctuating forces on a rigid circular cylinder in confined flow. *J. Fluid Mech.*, 78:561–576, 1976.

[29] W. Rodi. Comparison of LES and RANS calculations of the flow around bluff bodies. *J. Wind Ind. Aerodyn.*, 69-71:55–75, 1997.

[30] W. Rodi. Large-Eddy Simulation and statistical turbulence models: Complementary approaches. In O. Métais and J. Ferziger, editors, *New Tools in Turbulence Modelling*, Les Éditions de Physique, pages 49–72. Springer, 1997.

[31] W. Rodi, J.H. Ferziger, M. Breuer, and M. Pourquié. Status of large eddy simulation: Results of a workshop. *J. Fluid Eng.*, 119:248–262, 1997.

[32] P. Rollet-Miet. Simulation des grandes échelles a partir du code N3S: Ecoulement en canal. Technical Report HE-41/97/036/A, EDF, Chatou, France, 1997.

[33] G. Schewe. On the force fluctuations acting on a circular cylinder in crossflow from subcritical up to transcritical Reynolds numbers. *J. Fluid Mech.*, pages 265–285, 1983.

[34] H. Schlichting. *Grenzschichttheorie*. Braun, 1958.

[35] S. Sebag, V. Maupu, and D. Laurence. Non–orthogonal calculation procedures using second moment closure. In *Eighth Symposium on Turbulent Shear Flows, Munich*, pages 20.3.1–20.3.6. 1991.

[36] O. Simonin and M. Barcouda. Measurements and prediction of turbulent flow entering a staggered tube bundle. Fourth Int. Symp. on App. of Laser Anemometry to Fluid Mechanics, Lisbon, Portugal, 1988.

[37] J. Son and T.J. Hanratty. Velocity gradients at the wall for flow around a cylinder at Reynolds numbers from 5×10^3 to 10^5. *J. Fluid Mech.*, pages 353–368, 1969.

[38] S. Szepessy and B.W. Bearman. Aspect ratio and end plate effects on vortex shedding from a circular cylinder. *J. Fluid Mech.*, pages 191–217, 1992.

[39] T. Wei and C.R. Smith. Secondary vortices in the wake of circular cylinders. *J. Fluid Mech.*, 169:513–533, 1986.

[40] H. Werner and H. Wengle. Large–Eddy Simulation of turbulent flow over and around a cube in a plane channel. In U. Schumann et al., editor, *8th Symp. on Turb. Shear Flows*, 1993.

[41] G.S. West and C.J. Apelt. Fluctuating lift and drag forces on finite lengths of a circular cylinder in the subcritical Reynolds number range. *Journal of Fluids and Structures*, 11:135–158, 1997.

[42] M.M. Zdravkovich. *Flow Around Circular Cylinders*. Oxford University Press, 1997.